Polarizabilities of the 87Sr Clock Transition

C Shi, J.-L Robyr, U Eismann, M Zawada, L Lorini, R Le Targat, J Lodewyck

Polarizabilities of the ^{87}Sr Clock Transition

C. Shi,[1] J.-L. Robyr,[1] U. Eismann,[1] M. Zawada,[1,2] L. Lorini,[1,3] R. Le Targat,[1] and J. Lodewyck[1]

[1] *LNE-SYRTE, Observatoire de Paris, CNRS, UPMC ; 61 avenue de l'Observatoire, 75014 Paris, France*
[2] *Institute of Physics, Faculty of Physics, Astronomy and Informatics, Nicolaus Copernicus University, Grudziądzka 5, PL-87-100 Toruń, Poland*
[3] *Istituto Nazionale di Ricerca Metrologica (INRIM), Strada delle Cacce 91, 10135 Torino, Italy*

In this paper, we propose an in-depth review of the vector and tensor polarizabilities of the two energy levels of the ^{87}Sr clock transition whose measurement was reported in [P. G. Westergaard *et al.*, Phys. Rev. Lett. **106**, 210801 (2011)]. We conduct a theoretical calculation that reproduces the measured coefficients. In addition, we detail the experimental conditions used for their measurement in two Sr optical lattice clocks, and exhibit the quadratic behaviour of the vector and tensor shifts with the depth of the trapping potential and evaluate their impact on the accuracy of the clock.

PACS numbers: 06.30.Ft, 42.62.Fi, 37.10.Jk

Introduction

Optical lattice clocks are now the most stable frequency references [1–3], and their accuracy is steadily improving towards 10^{-17} to 10^{-18} [3–6]. In these clocks the systematic effects due to the atomic motion are cancelled by trapping a large number of ultra-cold atoms (typically 10^4) in the Lamb-Dicke regime, using an optical lattice formed by a standing wave laser beam. A specificity of these optical clocks is the strong light shift induced by the intense trapping light. At the so-called "magic wavelength", for which the scalar polarizabilities of the fundamental and excited clock states are identical, this light shift is largely suppressed [7]. However, in order to achieve a high accuracy, the residual polarization-dependent and higher order light shifts have to be evaluated. In reference [8], we reported exhaustive measurements of these light shifts with two ^{87}Sr lattice clocks, and showed that they are compatible with an accuracy of 10^{-17} at a trapping potential of 100 recoil energies. We reported the first experimental resolution of the vector-, tensor-, and hyper-polarizability and put an upper bound on higher order effects for ^{87}Sr.

In this paper, we focus on the first-order electric dipole interaction to propose a theoretical study of the coefficient of the decomposition of its Hamiltonian in vector and tensor irreducible operators that can reproduce the experimental results reported in [8]. The first section introduces the irreducible operator formalism describing the atomic polarizability. In the second section, we make use of this decomposition to theoretically evaluate the vector and tensor polarizability coefficients. The last section details the measurement of these coefficients and show their agreement with the theoretical estimates. Finally, we describe the non-linear dependence of the vector and tensor shifts with the depth of the trapping potential. Furthermore, we report on precise measurements of the magic wavelength and its sensitivity that provides insight in the physical properties of electronic levels of ^{87}Sr that are useful for characterizing the clock accuracy [9].

I. FACTORIZATION OF THE POLARIZABILITY OPERATOR

The Hamiltonian that describes an atomic level $|\phi\rangle = |nJFm\rangle$ in the presence of the electromagnetic field of a trapping light and a static bias magnetic field $\vec{B}_s$ reads:

$$\hat{H} = \hat{H}_Z + \hat{H}_{\text{eff}}. \tag{1}$$

$\hat{H}_Z$ is the Hamiltonian representing the Zeeman interaction:

$$\hat{H}_Z = \frac{g\mu_B}{\hbar}\hat{\vec{F}} \cdot \vec{B}_s, \tag{2}$$

where g is the Landé factor and μ_B the Bohr magneton. $\hat{H}_{\text{eff}}$ is the effective Hamiltonian representing the the off-resonant electric dipole interaction between the atom and the trapping light of complex amplitude $\mathcal{E}$ or power density $\mathcal{I} = \varepsilon_0 c|\mathcal{E}|^2/2$ in second-order perturbation theory [10]:

$$\hat{H}_{\text{eff}} = -\frac{1}{4}\hat{\alpha}|\mathcal{E}|^2, \tag{3}$$

where the polarizability operator $\hat{\alpha}$ reads:

$$\hat{\alpha} = \frac{1}{\hbar}\sum_{|\phi'\rangle} \frac{\vec{\varepsilon}^* \cdot \hat{\vec{d}}|\phi'\rangle\langle\phi'|\vec{\varepsilon} \cdot \hat{\vec{d}}}{\omega_0 - \omega_l} + \frac{\vec{\varepsilon} \cdot \hat{\vec{d}}|\phi'\rangle\langle\phi'|\vec{\varepsilon}^* \cdot \hat{\vec{d}}}{\omega_0 + \omega_l}, \tag{4}$$

where the sum runs over all excited states $|\phi'\rangle = |n'J'F'm'\rangle$. $\hat{\vec{d}}$ is the electric dipole operator, $\hbar\omega_0$ is the energy difference between $|\phi'\rangle$ and $|\phi\rangle$, and ω_l and $\vec{\varepsilon}$ are the angular frequency and polarization of the trapping light, respectively. Because the two states involved in the clock transition ($5s^2\ {}^1S_0$ and $5s5p\ {}^3P_0$, as show in figure 1) both have $J = 0$, their respective polarizabilities do not *a priori* depend on the magnetic sub-level m considered. However, the hyperfine Hamiltonian describing odd Sr isotopes with a non-zero nuclear spin slightly breaks the rotational invariance and introduces a minute dependence of the polarizabilities of ${}^1S_0$ and ${}^3P_0$ on m

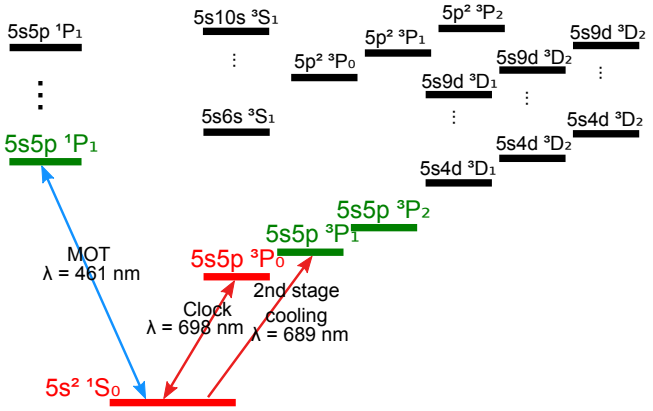

FIG. 1: Energy levels for Sr. The two clocks states are represented in red. The $F = 9/2$ hyperfine component of the three green states are involved in the vector and tensor polarizabilities of the excited clock state $5s5p\ ^3P_0$, as explained in section II. The other states are considered to calculate the polarizability coefficients of the clock transition.

and $\vec{\varepsilon}$. This dependence can be made analytically explicit by expanding the polarizability operator as the sum of three irreducible operators [11, 12]. In the $(2F+1)$-dimensional basis $|m\rangle \equiv \{|nJFm\rangle, -F \leq m \leq F\}$ of the hyperfine manifold of the Hilbert space describing either clock state, the matrix elements of this expansion read:

$$\langle m_2|\hat{\alpha}|m_1\rangle = \sum_{j=0}^{2} K_j \sum_{M=-j}^{j} (-1)^M C^{Fm_2}_{Fm_1 j\,-M} [\vec{\varepsilon}\otimes\vec{\varepsilon}^*]_{jM}, \tag{5}$$

where the first sum runs over the tensor rank j. In this expression, the dependence in $\vec{\varepsilon}$ is exclusively contained in the tensor product $[\vec{\varepsilon}\otimes\vec{\varepsilon}^*]_{jM}$, the dependence in m in the Clebsch-Gordan coefficient $C^{Fm_2}_{Fm_1 j\,-M}$ and the dependence in $|\phi'\rangle$ in the coefficients:

$$K_j = \frac{1}{\hbar} \sum_{|n'J'F'\rangle} k_j \left(\frac{1}{\omega_0 - \omega_l} + \frac{(-1)^j}{\omega_0 + \omega_l} \right), \tag{6}$$

where k_j is expressed using Wigner 6j-symbols and reduced dipole elements:

$$k_j = (-1)^{j-F-F'} \sqrt{\frac{2j+1}{2F+1}} \begin{Bmatrix} F & F & j \\ 1 & 1 & F' \end{Bmatrix} |(F'||d||F)|^2. \tag{7}$$

The canonical scalar α_s, vector α_v and tensor α_t polarizabilities are then defined by rescaling these coefficients:

$$\alpha_s = -\frac{1}{\sqrt{3}} K_0, \quad \alpha_v = \sqrt{\frac{2F}{F+1}} K_1, \quad \text{and} \quad \alpha_t = \sqrt{\frac{2F(2F-1)}{3(F+1)(2F+3)}} K_2. \tag{8}$$

These three physical parameters are sufficient to completely explicit the matrix of the polarizability operator given by equation (5). The first term of this equation, for $j = 0$, is the scalar polarizability. It is the main, rotationally invariant contribution to the polarizability. The vector polarizability ($j = 1$) appears only when $F \geq 1/2$ and when the light has a non-linear polarization. It is equivalent to a fictitious magnetic field along the light wave vector. It is an odd function of m, and accordingly vanishes when the light shift is averaged over opposite values of m. The last term ($j = 2$), appearing if $F \geq 1$, is the tensor polarizability that results in a polarization dependent polarizability with an even dependence in m.

The following section is devoted to the theoretical calculation of the three polarizability coefficients for the two atomic levels involved in the ^{87}Sr clock transition.

II. THEORETICAL CALCULATION OF THE POLARIZABILITIES

In order to further calculate the polarizabilities, the k_j coefficients can be related to the $|\phi'\rangle \to |\phi\rangle$ transition rate $\Gamma_{\phi\phi'}$, or to the radiative lifetime τ of the excited state $|\phi'\rangle$ through:

$$\frac{|(F'||d||F)|^2}{2F'+1} = B_{\text{hfs}} \frac{3\pi\varepsilon_0\hbar c^3}{\omega_0^3} \Gamma_{\phi\phi'} = B_{\text{hfs}} \frac{3\pi\varepsilon_0\hbar c^3}{\omega_0^3} B_{\text{fs}} \frac{\zeta}{\tau}, \tag{9}$$

where the fine and hyperfine branching ratios read:

$$B_{\text{fs}} = (2J+1)(2L'+1) \begin{Bmatrix} J' & 1 & J \\ L & S & L' \end{Bmatrix}^2, \tag{10}$$

$$B_{\text{hfs}} = (2F+1)(2J'+1) \begin{Bmatrix} F' & 1 & F \\ J & I & J' \end{Bmatrix}^2, \tag{11}$$

and ζ is a dimensionless parameter accounting for the fine structure splitting.

When neglecting the hyperfine interaction, the two states of the clock transition with $J = 0$ do not exhibit vector or tensor polarizabilities, as can be seen by setting $F = 0$ in equation (7). However, the hyperfine splitting of the excited states $|\phi'\rangle$:

$$\nu_{\text{hfs}} = \frac{1}{2}AC + B \frac{\frac{3}{4}C(C+1) - I(I+1)J'(J'+1)}{2I(2I-1)J'(2J'-1)}, \tag{12}$$

where $C = F'(F'+1) - I(I+1) - J'(J'+1)$ and A and B are magnetic dipole and electric quadrupole constants, gives rise to vector and tensor components. The relative magnitude of these latter components is expected to be on the order of the ratio between the hyperfine splitting ν_{hfs} and the frequency of the optical transitions $|\phi\rangle \to |\phi'\rangle$ [13]:

$$\frac{\alpha_{v,t}}{\alpha_s} \approx \frac{\nu_{\text{hfs}}}{\nu_{\text{optical}}}. \tag{13}$$

However, for a state $|\phi\rangle$ with $J = 0$, we can show that for any value of I, and with $J' = 1$ according to the electric

dipole selection rules:

$$\sum_{F'=I-J'}^{I+J'} k_2 C = 0 \qquad (J=0,\ J'=1), \tag{14}$$

such that the contribution of the magnetic dipole term A to the tensor polarizability is cancelled at first order in $\nu_{\rm hfs}$. Hence, the dominant contribution to the tensor shift is the quadrupole B, or the second order in $\nu_{\rm hfs}$, whichever is the largest. No such cancellation occurs for the vector shift. This property is particularly observed for ^{87}Sr, as the excited states with the largest hyperfine splitting feature $B \ll A$, like $5s6s\ ^3S_1$ and $5s5p\ ^3P_1$. As a consequence, their contribution to the tensor polarizabilities of the clock states is orders of magnitude smaller than what could be expected from (13).

Using experimental measurements of the lifetimes of excited states, completed by theoretical estimates of the strength of atomic transitions [14], we can calculate the dynamic polarizabilities for various states of ^{87}Sr at the magic wavelength ($\omega_l = 2\pi \times 368.6$ THz).

The scalar, vector and tensor polarizabilities of the fundamental state $5s^2\ ^1S_0$ are derived by summing over the excited states $5s5p\,^3P_1$ and $5skp\,^1P_1$ with $k = 5 \ldots 20$. They read, expressed in atomic units (a.u.):

$5s^2\ ^1S_0$		
α_s	α_v	α_t
279.8	4.75×10^{-5}	1.57×10^{-5}

(15)

The main contribution to the scalar polarizability comes from the $5s5p\,^1P_1$ state, while the vector and tensor terms are dominated by the $5s5p\,^1P_1$ and $5s5p\,^3P_1$ states. As expected, the ratio between the vector (resp. tensor) polarizability and the scalar polarizability is on the order of 10^{-7}, comparable with the ratio between magnetic dipole term A – about 200 MHz (resp. the quadrupole term B – about 50 MHz) and optical frequencies – about 500 THz.

The polarizability of the $5s5p\,^3P_1(F = 9/2)$ is estimated by summing over the $5sks\,^3S_1$ states with $k = 6 \ldots 10$, the $5p^2\,^3P$ states and the $5skd\,^3D$ states with $k = 4 \ldots 9$:

$5s5p\,^3P_1(F=9/2)$		
α_s	α_v	α_t
304.4	−50.3	−101.2

(16)

As expected from the fact that $J \neq 0$ for $^3P_1$, the vector and tensor polarizabilities are on the same order of magnitude as the scalar polarizability. Figure 2 confronts these numerical values to the experimental spectroscopy of the $5s^2\ ^1S_0 \rightarrow 5s5p\,^3P_1(F = 9/2)$ inter-combination line.

In the case of the excited clock state $5s5p\ ^3P_0$, a direct calculation is not sufficient because state mixing with the $5s5p\ ^3P_1(F = 9/2)$, $5s5p\ ^3P_2(F = 9/2)$ and $5s5p\ ^1P_1(F = 9/2)$ states alters its physical properties.

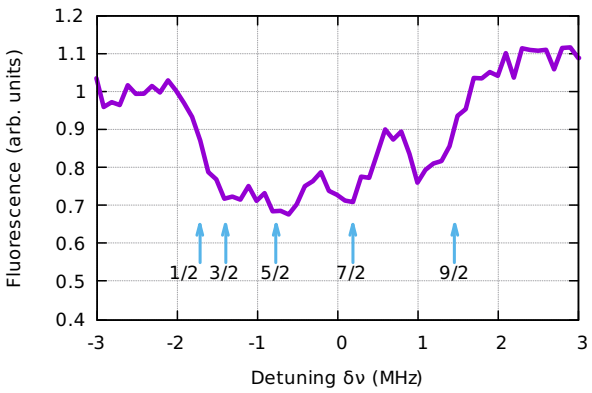

FIG. 2: Spectroscopy of the saturated $5s^2\ ^1S_0 \rightarrow 5s5p\,^3P_1(F = 9/2)$ transition by depletion of ^{87}Sr atoms in an optical lattice, for a linearly polarized trapping light, no magnetic field, and a trap depth of 1520 E_R, where $E_R = h \times 3.47$ kHz is the recoil energy associated with the absorption of a lattice photon with frequency ω_l. In this configuration, the polarizability operator (5) is already diagonal when choosing the quantization axis along the lattice polarization. Its eigen-values are $\alpha(m) = \alpha_s + \alpha_t \frac{3m^2 - F(F+1)}{F(2F-1)}$. The graph is centred on the light shift free frequency of the transition, and displays the splitting between magnetic sub-levels induced by the scalar and tensor polarizabilities of both states. The arrows indicate the theoretical light shift $\delta\nu = -\frac{1}{4}\alpha(m)|\mathcal{E}|^2$ for each value of $|m|$, as calculated from equations (15) and (16).

Since these states have $J \neq 0$, their vector and tensor polarizabilities are large and may contribute to the polarizabilities of the $^3P_0$ state. This state mixing is written:

$$|\phi\rangle = \sum_p c_p |\phi_p\rangle_0, \tag{17}$$

where the coefficients c_p are [15]:

$\lvert\phi_p\rangle_0$	$5s5p\ ^3P_0$	$5s5p\ ^3P_1$ $(F=9/2)$	$5s5p\ ^3P_2$ $(F=9/2)$	$5s5p\ ^1P_1$ $(F=9/2)$
c_p	1.	2.3×10^{-4}	-1.38×10^{-6}	-4.1×10^{-6}

(18)

When state mixing is involved, expanding the matrix elements of the polarizability operator (4) is more involving, but the result is that equations (5) through (11) remain valid expressions of these matrix elements, provided they are averaged over all $(|\phi_p\rangle_0, |\phi_q\rangle_0)$ combinations with a weight $c_p c_q^*$, and provided the branching ratios are replaced by:

$$\begin{aligned} \bar{B}_{\rm fs} &= (-1)^{S_p+S_q+2L'+J_p+J_q}\sqrt{(2J_p+1)(2J_q+1)} \\ &\times (2L'+1)\begin{Bmatrix} J' & 1 & J_p \\ L & S & L' \end{Bmatrix}\begin{Bmatrix} J' & 1 & J_q \\ L & S & L' \end{Bmatrix}, \end{aligned} \tag{19}$$

$$\bar{B}_{\rm hfs} = (2F+1)(2J'+1)\begin{Bmatrix} F' & 1 & F \\ J_p & I & J' \end{Bmatrix}\begin{Bmatrix} F' & 1 & F \\ J_q & I & J' \end{Bmatrix}. \tag{20}$$

Using these expressions, we can show that for $J_p = 0$ and $J_q = 1$, $\sum_{F'=|I-J'|}^{I+J'} k_2 = 0$ such that this combination has a negligible contribution to the tensor shift, and for $J_p = 0$ and $J_q = 2$, $\sum_{F'=|I-J'|}^{I+J'} k_1 = 0$ such that this second combination has a negligible contribution to the vector shift.

Among all the $(|\phi_p\rangle_0, |\phi_q\rangle_0)$ combinations involving the states listed in the table of equation (18), only a few lead to a non-negligible contribution. They are listed in bold characters in the following table:

$5s5p\,^3P_0$				
$\|\phi_p\rangle_0$	$\|\phi_q\rangle_0$	α_s	α_v	α_t
$^3P_0$	$^3P_0$	**288.8**	$\mathbf{9.3 \times 10^{-3}}$	1.9×10^{-6}
$^3P_1$	$^3P_1$	2×10^{-5}	2.7×10^{-6}	$\mathbf{-5.4 \times 10^{-6}}$
$^3P_0$	$^3P_1$	2×10^{-6}	$\mathbf{1.82 \times 10^{-1}}$	-1.5×10^{-6}
$^3P_0$	$^3P_2$	$\leq 10^{-13}$	-1.8×10^{-8}	$\mathbf{3.70 \times 10^{-4}}$
	Total	288.8	1.91×10^{-1}	3.65×10^{-4}

(21)

In this table, the $(|\phi_p\rangle_0, |\phi_q\rangle_0)$ and $(|\phi_q\rangle_0, |\phi_p\rangle_0)$ contributions for $p \neq q$ are grouped together. As expected from the theoretical considerations above, the tensor term of the $(^3P_0, ^3P_0)$ configuration is negligible, and the main contribution to the vector and tensor polarizabilities respectively come from the mixing combinations $(^3P_0, ^3P_1)$ and $(^3P_0, ^3P_2)$.

To express these polarizabilities in units more adapted to experimental purposes, we note $U_0 = \frac{1}{4}\alpha_s|\mathcal{E}|^2$ the trap depth. At the magic wavelength, α_s and hence U_0 are by definition identical for the two clock states. The numerical values of α_s shown in equations (15) and (21) show that this fact is approximately rendered by our calculation, which also gives an order of magnitude of a few percent for its accuracy, arising from uncertainties on the decay rates from excited states. For the vector and tensor polarizabilities, we introduce the coefficients:

$$\kappa^v = -\frac{\alpha_v}{\alpha_s}\frac{1}{h}\frac{1}{2F} \quad \text{and} \quad \kappa^t = -\frac{\alpha_t}{\alpha_s}\frac{1}{h}\frac{1}{2F(2F-1)}. \tag{22}$$

The following table gathers the theoretical values for κ^v and κ^t for the two clock states, as well as their difference $\Delta\kappa^{v,t} = \kappa^{v,t}(^3P_0) - \kappa^{v,t}(^1S_0)$:

$\|\phi\rangle$	κ^v (mHz/E_R)	κ^t (μHz/E_R)
$^3P_0$	-255	-60.9
$^1S_0$	-6.5×10^{-2}	-2.7
$\mathbf{^3P_0 - {}^1S_0}$	$\mathbf{-255}$	$\mathbf{-58.2}$

(23)

III. EXPERIMENTAL DETERMINATION OF THE POLARIZABILITIES

During the clock operation, a static bias magnetic field is applied to split the magnetic sub-levels. The energy levels are then the eigenvalues of the full Hamiltonian written in equation (1). Because $\hat{\vec{F}}$ is a vector operator, the Zeeman Hamiltonian adds up to the vector component of the polarizability operator. Therefore, the vector component of the Hamiltonian is equivalent to the action of an effective magnetic $\vec{b}_{\text{eff}}$ field equal to the vector sum of the static magnetic field $\vec{B}_s$ and the fictitious magnetic field that represents the vector light shift (see figure 3):

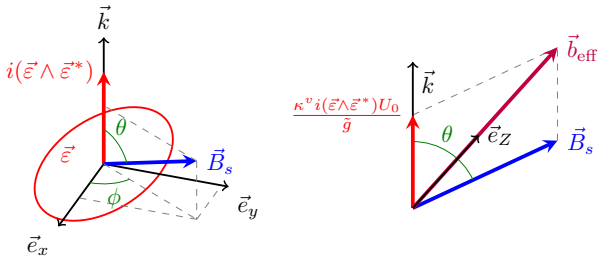

FIG. 3: Left: parametrization of the light polarization $\vec{\varepsilon}$ and the static bias magnetic field $\vec{B}_s$. $\vec{e}_x$ (resp. $\vec{e}_y$) is a unit vector along the major (resp. minor) axis of the trapping light polarization $\vec{\varepsilon}$, such that the polarization ellipsis (red) is included in the $(\vec{e}_x, \vec{e}_y)$ plane. Right: projection in the plane defined by the trapping light wave vector $\vec{k}$ and $\vec{B}_s$. The fictitious magnetic field representing the vector light shift adds to $\vec{B}_s$ to form an effective magnetic field $\vec{b}_{\text{eff}}$. If the vector component of the Hamiltonian dominates its tensor component, the Hamiltonian is diagonal for a quantization axis $\vec{e}_Z$ defined along $\vec{b}_{\text{eff}}$. When the polarization $\vec{\varepsilon}$ is elliptical, the quantization axis therefore depends on the trap depth U_0, introducing non-linear effects in the Zeeman shift and average clock frequency as a function of U_0.

$$\vec{b}_{\text{eff}} = \frac{\kappa^v i(\vec{\varepsilon}\wedge\vec{\varepsilon}^*)U_0}{\tilde{g}} + \vec{B}_s, \tag{24}$$

where $\tilde{g} = g\mu_B/h$. If the quantization axis $\vec{e}_Z$ is chosen along the effective magnetic field (*i.e* $\vec{e}_Z = \vec{b}_{\text{eff}}/||\vec{b}_{\text{eff}}||$), the vector component of the Hamiltonian is diagonal in the basis $\{|m\rangle, -F \leq m \leq F\}$ of eigen-vectors of F_Z. However, the tensor part of the Hamiltonian is *a priori* not diagonal in this basis. Yet, since $\kappa^v \gg \kappa^t$, if we assume that the bias field is large enough for the Zeeman splitting to be much larger than the energy splitting due to the tensor shift (For a trap depth $U_0 \sim 100\,E_R$, this assumption is satisfied if $B_s \gg 1$ μT), the states $\{|m\rangle\}$ remain approximate eigen-states of the full Hamiltonian. Expanding the tensor product in equation (5) then yields the energy shift $\delta\nu$ of level $|m\rangle$ of a given hyperfine manifold:

$$\delta\nu(m) = -\frac{U_0}{h} + m\tilde{g}||\vec{b}_{\text{eff}}|| + \kappa^t\beta U_0, \tag{25}$$

with

$$\beta = (3|\vec{\varepsilon}\cdot\vec{e}_Z|^2 - 1)(3m^2 - F(F+1)). \tag{26}$$

The middle term of equation (25) includes both the vector light shift and the Zeeman shift. It can be isolated

from the scalar and tensor terms by measuring the half difference $Z_s(m) = \frac{1}{2}(\delta\nu(m) - \delta\nu(-m))$ between opposite magnetic sub-levels:

$$Z_s = m\tilde{g}||\vec{b}_{\text{eff}}|| = m\sqrt{(\tilde{g}B_s\cos\theta + \kappa^v\xi U_0)^2 + (\tilde{g}B_s\sin\theta)^2}, \quad (27)$$

where $\xi = ||i(\vec{\varepsilon}\wedge\vec{\varepsilon}^*)||$ is the degree of circular polarization of the trapping light, and θ is the angle between the wave vector $\vec{k}$ and the bias field $\vec{B}_s$ (as shown on figure 3). The Taylor expansion of the later equation to second order in U_0 yields:

$$Z_s \simeq m\tilde{g}B_s + m\kappa^v\xi\cos\theta\, U_0 + m\sin^2\theta\frac{(\kappa^v\xi)^2}{2\tilde{g}B_s}U_0^2. \quad (28)$$

To experimentally evaluate the differential vector polarizability coefficient $\Delta\kappa^v$, we measured $\Delta Z_s = Z_s(^3P_0) - Z_s(^1S_0)$ for different trapping depths with $m = \pm 9/2$ and a circular polarization for the trapping light ($|\xi| = 1$). From these data we extrapolated the derivative of the Zeeman shift at zero trap depth $\partial\Delta Z_s/\partial U_0(U_0 = 0) = m\Delta\kappa^v\xi\cos\theta$. The trap depth is measured by observing the longitudinal motional side-bands of the trapped atoms [16]: their spacing and shape give a direct measurement of the trap depth (at the trap centre) and of longitudinal and transverse temperatures of the atoms [17]. From these three parameters, we can deduce the average trap depth experienced by the atoms.

Repeating the experiment for various values of θ enables to deduce the differential coefficient, as reported in [8]:

$$|\Delta\kappa^v| = 0.22 \pm 0.05\ \text{Hz}/E_R, \quad (29)$$

in agreement with the theoretical estimate reported in equation (23). The uncertainty is limited by the knowledge of the polarization state $\vec{\varepsilon}$ in the lattice cavity. In the usual clock operation, $\vec{B}_s$ is orthogonal to the wave vector $\vec{k}$ (*i.e.* $\cos\theta \simeq 0$). This configuration minimizes the first order term of equation (28), but it also maximizes its quadratic term. This latter term can therefore easily be observed, even for moderate trapping depths below 200 E_R. Figure 4 shows such a quadratic dependence for an elliptical polarization. In order to fit the data points of this figure, the two Landé factors of $^3P_0$ and $^1S_0$ have to be known. We performed a precise measurement of the ratio between these coefficients by locking the clock on $\sigma^{\pm}$ and π transitions, as shown on figure 5:

$$\frac{\tilde{g}(^3P_0)}{\tilde{g}(^1S_0)} = 1.58794(7). \quad (30)$$

Given the Landé factor of the fundamental state $\tilde{g}(^1S_0) = 184.4(1)$ [15, 18], this gives:

$$\tilde{g}(^3P_0) = 2.928(2)\text{MHz/T}, \text{ and } \Delta\tilde{g} = 1.0842(7)\text{MHz/T}. \quad (31)$$

in agreement with previously reported values [15].

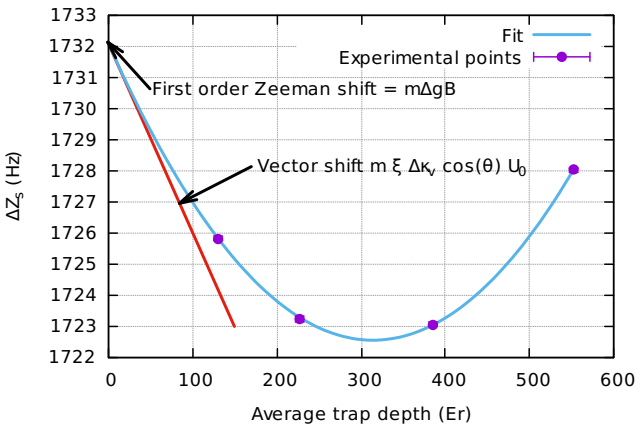

FIG. 4: Differential Zeeman shift ΔZ_s of the ^{87}Sr clock resonance as a function of the trap depth U_0 for an elliptical polarization $|\xi| \simeq 0.9$ and $|m = 9/2|$. The experimental data points are fit with equation (27), assuming $\kappa^v(^1S_0) = 0$. These four data points are sufficient to determine the three free parameters of this equation that describe the geometry of the experimental setup, here $B_s = 355.0 \pm 0.2$ μT, $\xi\kappa^v(^3P_0) = 212 \pm 2$ mHz/E_R, and $\theta = 63.9 \pm 0.5$ mrad.

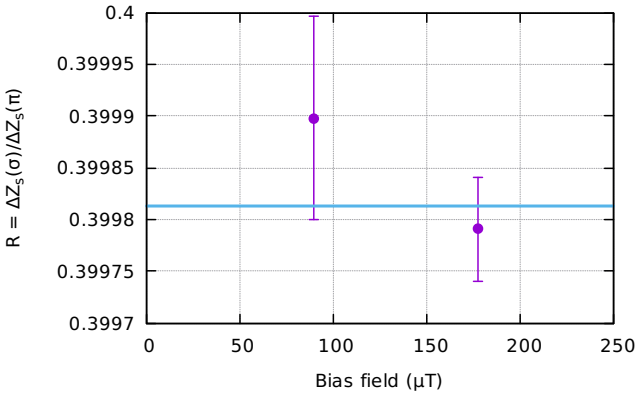

FIG. 5: Ratio R between the differential Zeeman shifts ΔZ_s (for linear polarization, so that no dependence in U_0 is observed) for $\sigma(|m| = 9/2 \rightarrow |m| = 7/2)$ and $\pi(|m| = 9/2 \rightarrow |m| = 9/2)$ transitions. This ratio is related to the ratio between Landé factors by $\tilde{g}(^3P_0)/\tilde{g}(^1S_0) = 9(R-1)/(9R-7)$.

The measurement of the tensor shift was conducted with a purely linear polarization for the trapping light, and therefore with a quantization axis along the bias field $\vec{B}_s$. The tensor component is extracted by measuring the average clock frequency shift for various values of β. The results are reported in table I:

$$\begin{aligned}\Delta\nu &= \frac{\nu(^3P_0,m) - \nu(^1S_0,m) + \nu(^3P_0,-m) - \nu(^1S_0,-m)}{2} \\ &= (\Delta\kappa^s + \beta\Delta\kappa^t)U_0. \end{aligned} \quad (32)$$

where:

Meas. #	1	2	3	4	5	6	7	8	9	10	11	12	13
$\sin\theta$	1	1	0.92	0.92	1	1	1	1	0.99	0.99	0.955	0.955	1
$\cos\phi$	0.602	0.602	0.602	0.602	0	0	1	1	1	1	1	1	0
m	9/2	7/2	9/2	7/2	9/2	7/2	9/2	7/2	9/2	7/2	9/2	7/2	9/2
β	3.12	1.04	-2.96	-0.99	-36	-12	72	24	70.0	23.3	63.05	21.0	-36

TABLE I: Geometrical configurations chosen to measure the tensor shift. A strictly linear polarization is selected by the enhancement cavity of the optical lattice by using an intra-cavity birefringent element. For this polarization, the β coefficient reduces to $\beta = (3\sin^2\theta\cos^2\phi - 1)(3m^2 - F(F+1)) = (3\cos^2 - 1)\alpha(3m^2 - F(F+1))$ where α is the angle between the polarization and the bias field $\vec{B}_s$. We switch between $\cos\phi = 1$ and $\cos\phi = 0$ by changing the polarization eigen-mode of the lattice cavity. The angles are derived from the relative values of the Zeeman shift when the magnetic field is changed.

$$\Delta\kappa^s = -\frac{\Delta\alpha_s}{\alpha_s} = -\frac{\alpha_s(^3P_0) - \alpha_s(^1S_0)}{\alpha_s} \tag{33}$$

is the remaining differential scalar light shift due to a possible detuning of the trapping light from the magic wavelength. The resulting value for the tensor shift coefficient is then, as reported in [8]:

$$\Delta\kappa^t_{\rm exp} = \frac{\partial\Delta\nu}{\partial\beta} = (-57.7 \pm 2.3)\,\mu{\rm Hz}/E_r, \tag{34}$$

in agreement with the theoretical value shown in equation (23) well within the experimental error bar.

We now consider the behaviour of the tensor light shift when the light polarization $\vec{\varepsilon}$ is not perfectly linear. In this case, the quantization axis $\vec{e}_Z$ for the excited state $^3P_0$ is aligned with the effective magnetic field $\vec{b}_{\rm eff}$ and thus varies with the trap depth U_0. Consequently, the β coefficient depends on U_0 through:

$$|\vec{\varepsilon}\cdot\vec{e}_Z|^2 = \left|\frac{\vec{\varepsilon}\cdot\vec{B}_s}{||\vec{b}_{\rm eff}||}\right|^2 \simeq |\vec{\varepsilon}\cdot\vec{e}_{B_s}|^2\left(1 - 2\frac{\kappa^v\xi\cos\theta\,U_0}{\tilde{g}B_s} + o\,(U_0)\right). \tag{35}$$

where $\vec{e}_{B_s}$ is the unit vector along $\vec{B}_s$. Because of this coupling effect between the vector and tensor light shifts, the average clock frequency contains a frequency shift $\Delta\nu_{vt}$ quadratic with the trapping potential reading:

$$\Delta\nu_{vt} = -\gamma_{vt}|\vec{\varepsilon}\cdot\vec{e}_{B_s}|^2\xi\cos\theta\,U_0^2, \tag{36}$$

with

$$\gamma_{vt} = \left(3m^2 - F(F+1)\right)\frac{6\kappa^t(^3P_0)\kappa^v(^3P_0)}{\tilde{g}(^3P_0)B_s}, \tag{37}$$

assuming that $^1S_0$ exhibits no vector shift. For ^{87}Sr we have $\gamma_{vt} = 11\ \mu{\rm Hz}/E_R^2$ for $B_s = 0.1$ mT. This quadratic frequency shift on the average clock frequency is three orders of magnitude smaller than the quadratic term of the Zeeman shift written in equation (28). But this effect is quite significant when compared to the hyperpolarizability coefficient $\gamma = 0.4\ \mu{\rm Hz}/E_R^2$ [8, 19]. However, it is dramatically reduced when the polarization is linear, $\vec{B}_s \perp \vec{k}$ and $\vec{B}_s \perp \vec{\varepsilon}$. Its experimental demonstration is for now challenging, as it is predominant in a configuration where the vector light shift is large and blurs the atomic resonances.

Finally, repeated measurements of the total light shift over two years with our two strontium clocks [5] confirmed the experimental value for the magic wavelength published in [8], for which the differential scalar light shift is cancelled (*i.e.* $\Delta\kappa^s = 0$):

$$\nu_{\rm magic} = 368\,554\,725 \pm 3\ {\rm MHz}. \tag{38}$$

The uncertainty on this value is limited by our knowledge of β used to subtract the tensor light shift from the total light shift from equation (32). In addition, we measured the sensitivity of the scalar light shift with the trapping light frequency $\nu_{\rm latt}$:

$$\frac{\partial\Delta\kappa^s}{\partial\nu_{\rm latt}} = -15.5 \pm 1.1\ \mu{\rm Hz}/E_R/{\rm MHz}. \tag{39}$$

This value is in agreement with the estimation given in [9] from Monte-Carlo simulation using transition strengths and scalar polarizabilities of the clock states at various frequencies.

Conclusion

In this paper, we have conducted a theoretical estimate of the vector and tensor polarizabilities of the ^{87}Sr clock states in agreement with experimental measurements. We have shown that the differential vector polarizability is largely due to state mixing of the excited clock state $^3P_0$ with $^3P_1$. The tensor polarizability is mainly due to state mixing of $^3P_0$ with $^3P_2$, with a small contribution from the hyperfine structure of $^1P_1$ on $^1S_0$. We also described a non-linear behaviour of these light shifts that are largely cancelled in normal clock operation, but that have to be considered as the accuracy of optical lattice clocks continues to improve.

SYRTE is UMR CNRS 8630 between Centre National de la Recherche Scientifique, Université Pierre et Marie Curie, and Observatoire de Paris. The Laboratoire National de Métrologie et d'Essais is the French National Metrology Institute. This work is supported by CNES, IFRAF and Nano-K-Conseil Régional Île-de-France and ESA under the SOC project.

[1] N. Hinkley, J. A. Sherman, N. B. Phillips, M. Schioppo, N. D. Lemke, K. Beloy, M. Pizzocaro, C. W. Oates, and A. D. Ludlow. An atomic clock with 10^{-18} instability. *Science*, 341(6151):1215–1218, 2013.

[2] C. Hagemann, C. Grebing, T. Kessler, S. Falke, N. Lemke, C. Lisdat, H. Schnatz, F. Riehle, and U. Sterr. Providing 10^{-16} short-term stability of a $1.5-\mu$m laser to optical clocks. *Instrumentation and Measurement, IEEE Transactions on*, 62(6):1556–1562, 2013.

[3] B. J. Bloom, T. L. Nicholson, J. R. Williams, S. L. Campbell, M. Bishof, X. Zhang, W. Zhang, S. L. Bromley, and J. Ye. An optical lattice clock with accuracy and stability at the 10^{-18} level. *Nature*, 506(7486):71–75, 2014.

[4] S. Falke, N. Lemke, C. Grebing, B. Lipphardt, S. Weyers, V. Gerginov, N. Huntemann, C. Hagemann, A. Al-Masoudi, S. Hfner, S. Vogt, U. Sterr, and C. Lisdat. A strontium lattice clock with 3×10^{-17} inaccuracy and its frequency. *New Journal of Physics*, 16(7):073023, 2014.

[5] R. Le Targat, L. Lorini, Y. Le Coq, M. Zawada, J. Guna, M. Abgrall, M. Gurov, P. Rosenbusch, D. G. Rovera, B. Nagrny, R. Gartman, P. G. Westergaard, M. E. Tobar, M. Lours, G. Santarelli, A. Clairon, S. Bize, P. Laurent, P. Lemonde, and J. Lodewyck. Experimental realization of an optical second with strontium lattice clocks. *Nature Communications*, 4:2109, 2013.

[6] I. Ushijima, M. Takamoto, M. Das, T. Ohkubo, and H. Katori. Cryogenic optical lattice clocks. *Nature Photonics*, 9:185, 2015.

[7] Hidetoshi Katori, Masao Takamoto, V. G. Pal'chikov, and V. D. Ovsiannikov. Ultrastable optical clock with neutral atoms in an engineered light shift trap. *Phys. Rev. Lett.*, 91:173005, Oct 2003.

[8] P. G. Westergaard, J. Lodewyck, L. Lorini, A. Lecallier, E. A. Burt, M. Zawada, J. Millo, and P. Lemonde. Lattice-induced frequency shifts in Sr optical lattice clocks at the 10^{-17} level. *Phys. Rev. Lett.*, 106:210801, 2011.

[9] T. Middelmann, S. Falke, C. Lisdat, and U. Sterr. High accuracy correction of blackbody radiation shift in an optical lattice clock. *Phys. Rev. Lett.*, 109:263004, 2012.

[10] C. Cohen-Tannoudji and J. Dupont-Roc. Experimental study of zeeman light shifts in weak magnetic fields. *Phys. Rev. A*, 5:968–984, 1972.

[11] M. V. Romalis and E. N. Fortson. Zeeman frequency shifts in an optical dipole trap used to search for an electric-dipole moment. *Physical Review A*, 59(6):4547, 1999.

[12] V D Ovsyannikov, Vitalii G Pal'chikov, H Katori, and M Takamoto. Polarisation and dispersion properties of light shifts in ultrastable optical frequency standards. *Quantum Electronics*, 36(1):3–19, 2006.

[13] H. Katori, M. Takamoto, V. G. Pal'chikov, and V. D. Ovsiannikov. Ultrastable optical clock with neutral atoms in an engineered light shift trap. *Physical Review Letters*, 91(17):173005, 2003.

[14] M. M Boyd. *High precision spectroscopy of strontium in an optical lattice: Towards a new standard for frequency and time*. PhD thesis, University of Colorado, 2007.

[15] M. M. Boyd, T. Zelevinsky, A. D. Ludlow, S. Blatt, T. Zanon-Willette, S. M. Foreman, and J. Ye. Nuclear spin effects in optical lattice clocks. *Physical Review A*, 76(2):022510, 2007.

[16] S. Blatt, J. W. Thomsen, G. K. Campbell, A. D. Ludlow, M. D. Swallows, M. J. Martin, M. M. Boyd, and J. Ye. Rabi spectroscopy and excitation inhomogeneity in a one-dimensional optical lattice clock. *Phys. Rev. A*, 80:052703, 2009.

[17] Rodolphe Le Targat. *Optical lattice clock with strontium atoms : a second generation of cold atom clocks*. Theses, Télécom ParisTech, July 2007.

[18] L. Olschewski. Messung der magnetischen Kerndipolmomente an freien ^{43}Ca-,^{87}Sr-,^{135}Ba-,^{137}Ba-,^{171}Yb- und ^{173}Yb-Atomen mit optischem Pumpen. *Zeitschrift für Physik*, 249(3):205–227, 1972.

[19] R. Le Targat et al. Comparison of Sr optical lattice clocks at the 10^{-16} level. *Proceedings of the EFTF*, 2012.